Synthesis of Cs-ABW nanozeolite in organotemplate-free system

Tamara Mahmoud Ali Ghrear, Séverinne Rigolet, T. Jean Daou, Svetlana Mintova, Tau Chuan Ling, Soon Huat Tan, Eng-Poh Ng

▶ To cite this version:

HAL Id: hal-02047590

https://normandie-univ.hal.science/hal-02047590

Submitted on 26 Nov 2020

Synthesis of Cs-ABW Nanozeolite in Organotemplate-free System

Tamara Mahmoud Ali Ghrear,[a] Severinne Rigolet,[b] T. Jean Daou,[b] Svetlana Mintova,[c] Tau Chuan Ling,[d] Soon Huat Tan,[e] Eng-Poh Ng[a,*]

[a]*School of Chemical Sciences, Universiti Sains Malaysia, 11800 USM, Penang, Malaysia.*

[b]*Université de Haute-Alsace, Université de Strasbourg, Axe Matériaux à Porosités Contrôlées, Institut de Science de Matériaux de Mulhouse UMR 7361, ENSCMu, 3b rue Alfred Werner, 68093 Mulhouse, France.*

[c]*Laboratoire Catalyse & Spectrochimie, ENSICAEN, Université de Caen, 14000 Caen, France.*

[d]*Institute of Biological Sciences, Faculty of Science, University of Malaya, 50603 Kuala Lumpur, Malaysia.*

[e]*School of Chemical Engineering, Engineering Campus, Universiti Sains Malaysia, Penang, Malaysia*

*Corresponding author. Tel: +6046533550; e-mail address: epng@usm.my

Abstract:

Cesium-aluminosilicate zeolite nanocrystals with ABW framework structure are synthesized free of organic template using hydrothermal approach. The crystallization process of Cs-ABW zeolite nanocrystals by varying the initial gel molar composition, heating temperature and crystallization time was studied. More detailed investigations of the formation of Cs-ABW nanozeolite using a reactive clear precursor hydrogel ($4SiO_2:1Al_2O_3:16Cs_2O:160H_2O$) were then carried out. Fully crystalline Cs-ABW nanozeolites were obtained within 120 min at 180 °C and 22 bar, which is considerably faster in comparison to the currently available method involving treatment at 695 °C, 1000 bar and 46 h. The Cs-ABW nanocrystals have grain shape morphology with a mean size of 32 nm and they do not agglomerate for long durations. The nanosized Cs-ABW zeolite has high alumina content (Si/Al ratio = 1.04). These nanocrystals

can be prepared in high solid yield (ca. 82%) thus offering a promising route for large-scale production of highly basic zeolite nanoparticles.

1.   Introduction

Zeolites are crystalline microporous aluminosilicates made from $[AlO_4]^{3-}$ and $[SiO_4]^{4-}$ tetrahedral units, forming channels and cavities. Zeolites are widely used in catalysis, ion exchange, adsorption and separation processes due to their high porosity, tunable acidity/basicity and high ion-exchange capacity [1-3]. Recently, a number of works has been reported on the synthesis, characterization and applications of zeolites with crystallite size below 100 nm due to their superior properties such as reducing diffusion path length, large external surface area, high colloidal stability, etc. [4-7].

Typically, zeolite nanocrystals are synthesized using organic templates (amine, imidazolium or quaternary ammonium salts) for controlling the crystallite size [8-10]. In addition, other more eco-friendly and cheaper approaches such as seed-induced [11, 12], ionothermal [13], post-milling recrystallization [14, 15], confined space synthesis [16] and organotemplate-free [17, 18] methods were used to prepare nanosized zeolite and zeotype materials. So far, a number of zeolite nanocrystals (*BEA [19], EDI [5], EMT [20], FAU [21, 22], GIS [23], LTA [24], LTJ [17], LTL [25], MEL [26], MER [27], MFI [28], MOR [29], SOD [30]) and zeotype (AEI [31], AFI [32], AFO [33], CHA [34]) has been successfully synthesized.

The zeolite of ABW topology with a framework composition of $LiAlSiO_4.2H_2O$ was first synthesized by Barrer and White in 1951 [35]. The ABW framework is constructed by 4-, 6- and 8-rings of TO_4 tetrahedral (T = Si, Al), forming one-dimensional 8-membered ring (8MR) channel system (diameter of 3.4×3.8 Å^2) [36]. Typically, ABW framework is preferentially formed in the hydrogels containing Li^+ cations (250 °C, 72 h) [37]. Furthermore, the formation of ABW zeolite templated by Cs^+ cation was also reported in 1970s (700-1200 °C, >1000 bar, 46 h) [38]. The synthesis condition of Cs-ABW has recently been improved to a much lower temperature and pressure (695 °C, 1000 bar) but the crystallization time was the same [39, 40]. As described, the synthesis of ABW-type zeolite still requires long crystallization time, extremely high temperature and pressure. Thus, ABW-type zeolites are rarely reported considering its tedious and dangerous synthesis condition. Also, nucleation and crystal growth of nanosized Cs-ABW zeolite has also not been reported so far and hence, it is the basis of this study.

In this work, Cs-ABW zeolite nanocrystals synthesized in template-free Al_2O_3–SiO_2–Cs_2O–H_2O precursor system are reported. The effects of zeolite synthesis parameters including initial molar composition of precursor mixture, temperature and crystallization time are firstly studied. Secondly, the crystal growth process of the ABW nanocrystals are studied in time-dependent experiment under mild and safe synthesis conditions (low temperature and pressure) compared to the previous works. The crystallization process of Cs-ABW nanocrystals is monitored using microscopic and spectroscopic methods.

2. Experimental

2.1. Hydrothermal synthesis of nanosized Cs-ABW zeolite

The nanosized Cs-ABW was prepared as follows: Firstly, clear aluminate solution was prepared by dissolving $CsOH.H_2O$ (3.500 g, Sigma-Aldrich) and $Al(OH)_3$ (0.414 g, Acros) in distilled water (2.688 g) at 105 °C for 16 h under continuous stirring (400 rpm). Next, a clear silicate solution was obtained by mixing HS-40 (1.594 g, Sigma-Aldrich) and $CsOH.H_2O$ (10.763 g) in distilled water (2.663 g) at room temperature for 10 min under stirring (400 rpm). The aluminate solution was then added slowly into the silicate solution under vigorous stirring (600 rpm) to obtain a clear precursor solution. The precursor sol with a molar composition of $4SiO_2:1Al_2O_3:16Cs_2O:164H_2O$ was stirred for another 5 min before transferring into a 15-mL Teflon autoclave for crystallization at 180 °C (10, 17, 30, 60 and 120 min). To ensure high reproducibility of the synthesis, the mass of autoclave before and after heating was recorded; negligible amount of water (<0.0020 g) was lost from the samples after the heating. The suspension was purified with distilled water (centrifuged at 10000 rpm, 15 min) until pH of 8 was reached prior to freeze drying. All experiments performed *via* varying the chemical compositions of the precursor mixtures and synthesis conditions are summarized in Table 1.

2.2.   *Characterization*

The crystallinity and purity of solids were investigated by a PANalytical X'Pert PRO diffractometer with Cu-K$_\alpha$ monochromatized radiation (λ = 1.5406 Å). The measurement was performed with a scan speed of 0.2°/min and a step size of 0.02°. The degree of crystallinity was estimated by evaluating the intensity of the three most intense XRD peaks of the samples at 2θ of 27.5° [202]/[112], 18.68° [200]/[110] and 32.89° [310]/[020], relative to the reference sample (Cs-ABW synthesized for 120 min). The crystallite size of the zeolite nanocrystals was estimated by using the Scherrer equation. The morphological features and the crystal size of amorphous particles and zeolite nanocrystals were examined using a Philips CM12 TEM

microscope operated at 200 kV. The particle size of the amorphous or crystal solids was measured by randomly counting of 50 particles through TEM images obtained in different areas. The infrared (IR) spectra of the solids were recorded with a Perkin Elmer spectrometer (System 2000) within the range of 1400–400 cm^{-1} using the KBr pellet technique (KBr:sample weight ratio = 50:1).

The chemical composition of samples was determined using a Varian Vista MPX ICP-OES spectrometer (the solids were dissolved in a HF solution (0.5 M); H_3BO_3 was then added into the prepared solution to avoid interferences of fluoride in the ICP-OES analysis). ^{29}Si (I = 1/2) proton decoupled magic angle spinning (MAS + DEC) NMR spectra were recorded at room temperature with a Bruker Avance II 300 MHz spectrometer operating at $B_0 = 7.2$ T (Larmor frequency $\nu_0 = 59.62$ MHz) equipped of a Bruker 7 mm double channels probe. The probe rotor was spun at a spinning frequency of 4 kHz. Single pulse magic angel spinning (SPE-MAS) experiments were performed using a pulse angle of $\pi/6$ (2.1 µs) and a recycling delay of 80 s under high-power proton decoupling conditions (63 MHz). The chemical shifts were quoted relative to tetramethylsilane (TMS). The decompositions of the spectra were performed using the DMFit software [41]. ^{27}Al (I = 5/2) magic angle spinning (MAS) NMR was carried out with a Bruker Avance II 400 spectrometer operating at $B_0 = 9.4$ T (Larmor frequency $\nu_0 = 104.2$ MHz) equipped with a Bruker 2.5 mm double channel probe. The rotor was spun at 25 kHz, and free induction decays (FID) were collected with a p/12 rf pulse (0.6 ms) and a recycle delay of 1 s. Measurements were carried out with $[Al(H_2O)_6]^{3+}$ as an external standard reference.

3. Results and discussion

3.1. Effect of synthesis parameters on the formation of ABW nanosized zeolite

The effects of the synthesis parameters such as the initial gel molar composition, heating temperature and crystallization time on the formation of Cs-ABW crystals were first investigated (Table 1). Various amounts of Cs_2O were used for the preparation of the initial mixture ($4SiO_2:1Al_2O_3:xCs_2O:164H_2O$), and then hydrothermal treatment was performed at 180 °C for 80 min (Table 1). It was found that the crystallization rate increased with increasing the Cs_2O content, thus indicating the direct participation of soluble Cs_2O species in crystal growth process. In addition, a reduction of crystallite size from 41 nm to 26 nm was observed with increasing the Cs_2O molar ratio from 12 to 16.

The influence of water content in the precursor mixture on the properties of the zeolites was studied as well. The XRD analysis revealed that all samples showed similar XRD patterns of ABW crystalline phase with slight different degree of amorphous matter present. Thus, it indicated that tuning water content had negligible effect on the purity of the crystalline phase but influenced the degree of crystallinity of the ABW zeolite. By the reducing water in the precursor mixture, the crystallite size decreased from 44 nm to 19 nm. Such phenomenon happened because the precursor with reduced water content and higher alkalinity has higher solubility towards silicate and aluminate monomers. As a result, a high super-saturation solution for the formation of small nanocrystals, by which many nucleation sites can produce, was formed [42].

The effect of SiO_2/Al_2O_3 ratio on the solid products formed was also studied. The XRD results showed that the crystallization rate was significantly affected by the silica content of the precursor mixture. When SiO_2/Al_2O_3 ratios of 2 and 4 were used, Cs-ABW nanocrystals with crystallite sizes of 34 nm and 26 nm were obtained, respectively. Further increasing the SiO_2/Al_2O_3 ratio to 6, however, yielded amorphous solid as end product.

In order to study the effect of Cs^+ cation in the formation of ABW framework, different types of metal hydroxide were used while the other synthesis parameters were constant ($4SiO_2:1Al_2O_3:16M_2O:164H_2O$, M = Na, K or Cs, 180 °C, 80 min). When NaOH and KOH were employed, the precursors did not yield ABW crystalline phase. Instead, CAN and LTJ framework structures were crystallized, respectively. Hence, Cs^+ plays an important role in governing the ABW phase selectivity during zeolite nucleation. The crystallite size of ABW zeolite (26 nm) was much smaller than LTJ (94 nm) and CAN (56 nm) zeolites. This phenomenon can be explained by the stronger alkalinity of CsOH than those of KOH and NaOH in enhancing the overall solubility of aluminate and silicate species promoting high super-saturation condition [43].

The precursor solution with a molar composition of $4SiO_2:1Al_2O_3:16Cs_2O:164H_2O$ were also subjected to heating at different temperatures (140, 160 and 180 °C) for 80 min in order to study the effect of heating on the formation of Cs-ABW material. As shown, only the ABW crystalline solid product was obtained at 180 °C while the other two solids heated at lower temperatures were mostly amorphous indicating that the crystallization of Cs-ABW zeolite was a thermally-activated process. The effects of heating time was also studied and the formation of Cs-ABW zeolite was found to be time-dependent. The formation of Cs-ABW zeolite nanocrystals as a function of crystallization time will be discussed in the following sections.

3.2. Kinetics of formation of Cs-ABW nanocrystals

The synthesis of nanocrystalline Cs-ABW zeolite was prepared by mixing both the transparent aluminate and silicate solutions. The resulting clear suspensions became more viscous indicating the polymerization of aluminate and silicate species. The precursor was then

subjected to hydrothermal treatment at 180 °C to induce further the crystallization. When this reactant sol was heated for 7 min, the sol remained clear and no solid product was recovered at this stage. However, an increase in the solubility of the alumina and silica precursors was observed, which allowed more precursor species to dissolve in the sol and hence increasing the critical supersaturation of the sol. After 10 min, the solution turned cloudy and a colloidal stable solution was obtained. The sample was separated and a soft gel was collected at the bottom of the centrifuge tubes. The mass of the solid product after purification and freeze drying was 28% (Fig. 1). According to the XRD analysis, this sample was an amorphous solid since no XRD diffraction peaks were detected and only a broad band at $2\theta = 27.2°$ was observed (Fig. 2a and 3). Small particles with irregular shape and particle size of 16 nm were detected by TEM (Fig. 4a,b). With further heating of the suspension (17 min), semi-hard solid product embedded in hydrogel was recovered under centrifugation. The solid yield at this stage increased to 34% (Fig. 1). Furthermore, the XRD pattern of this sample contains an amorphous hump and several diffraction peaks at $2\theta = 18.80°$, $26.94°$, $27.52°$, $32.90°$ and $38.78°$, which corresponded to the (200)/(110), (211), (202)/(112), (310)/(020) and (312)/(022) planes of the ABW-type zeolite, respectively (Fig. 2b) [39]. The diffraction peaks were broad indicating the small crystallite size of zeolite domains. The degree of crystallinity of this solid sample was also determined (Fig. 3). It was shown that the amorphous entities were still dominated in the sample; 18 % crystallinity was recorded. The XRD observation was supported by the TEM analysis. As shown in Fig. 4c,d, transformation of amorphous phase into the ABW zeolite nanocrystals was observed. The average crystal size of the ABW zeolite measured by TEM analysis is 17 nm and it was almost identical to that calculated from the Scherrer equation (15.2 nm).

The solid yield and the degree of crystallinity increased abruptly to 61% and 46.25%, respectively when the precursor was further heated to 30 min (Figs. 1 and 3). All the diffraction peaks became more intense while very weak amorphous hump remained weak (Fig. 2c). As

can be seen in the TEM images, the nanocrystals exhibited a grain shape which is different from that of Li-ABW micron-sized crystals (Fig. 4e,f) [44, 45]. Amorphous entity was still observed between the ABW nanocrystals. However, the amorphous solids slowly disappeared due to its consumption as a nutrient for the nucleation and crystal growth processes of zeolite nanocrystals. The particle size of the Cs-ABW nanocrystals was slightly increased to 25 nm (Scherer equation: 21 nm).

The colloidal suspensions subjected to further hydrothermal treatment for 60 and 120 min were purified. At these crystallization stage, the solid yield further increased and maintained at about 82% (Fig. 1). The XRD pattern of sample heated for 60 min contains more intense Bragg peaks, which correspond to samples with 83% crystallinity (Fig. 2d and 3). After 120 min, fully crystalline solid was obtained as indicated by XRD; the crystallite size of the ABW zeolite is about 28 nm (Fig. 2e). As shown, the XRD pattern of nanosized Cs-ABW zeolite is identical to that of Cs-ABW zeolite synthesized under high temperature and high pressure (Fig. 2f) [39]. The nanocrystals are well separated and the amorphous matter was transformed into Cs-ABW nanocrystals (32 nm, Fig. 4g,h). In comparison to the previous work (46 h) [38–40], the ABW nanocrystals were synthesized for shorter time thanks to the optimized precursor suspension used. In addition, the temperature (180 °C) and pressure (22 bar) used in the current study was much lower than those reported in the previous study (695–1200 °C, >1000 bar) [38–40].

Additionally spectroscopy techniques were used to follow the nucleation and crystallization processes of the ABW zeolite. Fig. 5 shows the IR spectra recorded from samples hydrothermally treated at different times. Only four IR bands were detected in the sample heated for 10 min: at 1113, 1019, 802 and 472 cm^{-1} which are typical for amorphous aluminosilicates (Fig. 5a) [5]. The IR spectrum of the sample heated for 17 min contain bands at 1009 and 1128 cm^{-1}, which were assigned to the internal vibrations of Si–O–T (T = Si, Al)

9

asymmetric stretching modes (Fig. 5b) [17]. On the other hand, another IR band at 1053 cm^{-1} assigned to the Si–O–T symmetric stretching vibration mode appeared [46]. The intensity of these bands increased in the samples subjected to longer crystallization and also a peak shifting was observed indicating the change of the chemical composition of the sample, i.e., increased of Al content (Fig. 5b-d). Additionally, several weak bands at 530, 547 and 604 and 666 cm^{-1}, which are characteristics of double zigzag chains (dzc) in the Cs-ABW zeolite, started to appear in the sample treated for 30 min [47]. This double zigzag chains are composed of 4-rings and when they are connected, an 8-ring channels are formed [48]. Thus, the presence of these four IR bands indicated that the crystalline Cs-ABW zeolite is formed. A weak band at 448 cm^{-1} corresponding to the TO$_4$ bending vibration was also detected, and it slightly shifted to 440 cm^{-1} for the sample treated for120 min (Fig. 5b) [46]. All of these IR characteristic bands became more pronounced upon increasing crystallization time and no change in the IR spectrum was observed after 120 min of crystallization showing that fully crystalline Cs-ABW had been obtained (Fig. 5c,d).

The chemical composition of the solid products was determined using ICP-OES spectroscopy. In general, the Si content decreased while the Al and Cs contents increased with increasing the crystallinity of the samples under prolonged heating time (Table 2). At 10 min, the Si/Al ratio was 11.28 indicating that self-polymerization among silicate species is more favorable than the aluminate species [49]. Furthermore, low Cs/Al ratio (0.35) was also measured due to the presence of merely amorphous Al anionic species unable electrostatically to bind with the Cs$^+$ cations [50]. At 17 min, the Si/Al ratio decreased drastically to 1.87 while the Cs/Al ratio increased to 0.71 suggesting that structure rearrangement and mass transformation of the amorphous into crystalline material are proceeding. The Si/Al ratio finally reached almost unity when fully crystalline Cs-ABW solids were obtained. Thus, the high alumina Cs-ABW zeolite nanocrystals had been obtained. The elemental composition of

the ABW nanocrystals is similar to the one reported by Gatta et al. [39]. According to Gatta et al., the Cs^+ cations are located off-center in the 8MR-channels as extra-framework species where staggering of Cs^+ cations can be well seen in projection onto the plane of the 6-MRs of tetrahedra.

The ^{27}Al solid state MAS NMR spectra of all samples were also recorded. The spectra contain a resonance peak at 56 ppm which is corresponding to Al species in tetrahedral coordination (Fig. 6). Since this is the coordination state of Al in both amorphous and zeolite phases, this result did not provide distinguished information about the samples with different degree of crystallinity. The peak centred at 55.4 ppm became more narrower in the sample after 17 min heating, indicating homogeneous surrounding of the Al species and high symmetry (Fig. 6b). On the other hand, the ^{28}Si MAS NMR spectra show more information concerning the environment of the Si species in amorphous, semi-crystalline and crystalline samples. For the solid obtained after 10 min of heating, an intense and broad signal centred at –111.2 ppm was detected indicating the presence of unreacted silica in the form of $Si(OSi)_4$ (Fig. 7a). Two smaller contributions were also observed at –100.4 ppm and –86.2 ppm. The first band could be attributed to the Q_4 groups $(Si(OSi)_3(OAl))$ and/or Q_3 groups $(Si(OSi)_3(OH))$, while the second band was attributed to Q_2 groups $(Si^-(OSi)(OAl)_3)$ and/or Q_3 groups $(Si(OAl)_2(OSi)(OH))$ [51]. Increasing the heating time to 17 min and above evidenced the disappearance of the resonance at –111.2 ppm and the appearance of a well-defined resonance centered at ca. –94 ppm (Fig.7b–d) which was attributed to Q_4 groups. This sharp peak corresponded to the unique Si crystallographic site of ABW framework. Another peak ca. –88 ppm was also observed for these three samples which was attributed to Q_3 groups $(Si(OAl)_2(OSi)(OH))$ thanks to $^1H–^{29}Si$ CPMAS experiments (results not shown). The intensity of this peak seemed to decrease while increasing the

heating time of the samples indicating a higher degree of crystallinity for the sample heated for 120 min compared to the other samples; these results are consistent with the XRD data.

4. Conclusions

In summary, the synthesis of nanosized ABW- type zeolite containing Cs^+ extra framework cations in hydrogel free of organic template is presented. From an environmental point of view, this synthesis is beneficial as the ABW nanosized zeolite can be prepared under mild pressure and temperature without using harmful organic template. The nanocrystalline Cs-ABW zeolite can be easily obtained within 120 min hydrothermal treatment at 180 °C without using any organic template and the synthesis condition is very mild as compared to that reported in previous works. The formation of nanosized Cs-ABW zeolite is initiated by oligomerization of alumina and silica units in precursor solution, followed by polymerization to form amorphous entities before nuclei formation, crystallization and crystal growth take place under prolonged crystallization time. The resulting nanocrystals have an average diameter of 32 nm and narrow particle size distribution. The work presented can be beneficial for catalytic and selective sorption applications since the zeolite nanocrystals contain high basicity, small pores and have high solid yield (>80%).

References

[1]   S.M. Al-Jubouri, S.M. Holmes, Chem. Eng. J. 308 (2017) 476-491.

[2]   G. Majano, E.-P. Ng, L. Lakiss, S. Mintova, Green Chem. 13 (2011) 2435-2440.

[3]   B. Liu, Z. Chen, J. Huang, H. Chen, Y. Fang, Micropor. Mesopor. Mater. 273 (2019) 235-242.

[4]   M. Rahimi, E.-P. Ng, K. Bakhtiari, M. Vinciguerra, H.A. Ahmad, H. Awala, S. Mintova, M. Daghighi, F.B. Rostami, M. de Vries, M.M. Motazacker, M.P. Peppelenbosch, M. Mahmoudi, F. Rezaee, Sci. Rep. 5 (2015) 17259.

[5]   S.-F. Wong, K. Deekomwong, J. Wittayakun, T.C. Ling, O. Muraza, F. Adam, E.-P. Ng, Mater. Chem. Phys. 196 (2017) 295-301.

[6]   G. Huang, P. Ji, H. Xu, J.-G. Jiang, P. Wu, Micropor. Mesopor. Mater. 248 (2017) 30-39.

[7]   B.A. Holmberg, X. Wang, Y. Yan, J. Membrane Sci. 320 (2008) 86-92.

[8]   E.-P. Ng, D.T.L. Ng, H. Awala, K.-L. Wong, S. Mintova, Mater. Lett. 132 (2014) 126-129.

[9]   S. Mintova, N.H. Olson, V. Valtchev, T. Bein, Science 283 (1999) 958-960.

[10]   W. Song, V.H. Grassian, S.C. Larsen, Chem. Commun. (2005) 2951-2953.

[11]   L. Shi, N. Li, L. Wang, R. Liu, Y. Li, Micropor. Mesopor. Mater. 258 (2018) 178-188.

[12]   Y. Kamimura, S. Tanahashi, K. Itabashi, A. Sugawara, T. Wakihara, A. Shimojima, T. Okubo, J. Phys. Chem. C 115 (2011) 744-750.
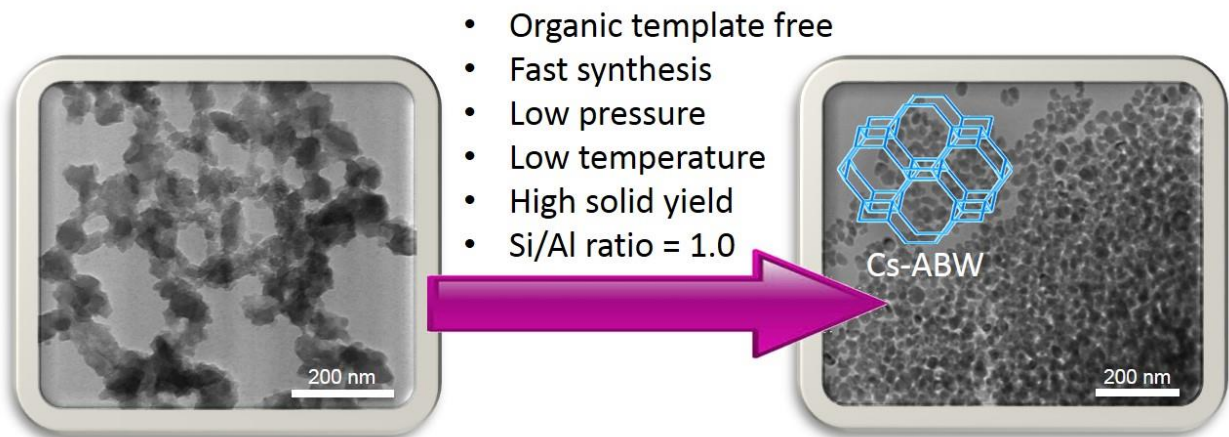
[13]   D.Y. Khoo, W.-M. Kok, R.R. Mukti, S. Mintova, E.-P. Ng, Solid State Sci. 25 (2013) 63-69.

[14]   T. Wakihara, R. Ichikawa, J. Tatami, A. Endo, K. Yoshida, Y. Sasaki, K. Komeya, T. Meguro, Cryst. Growth Des. 11 (2011) 955-958.

[15]   H. Yamada, T. Iida, Z. Liu, Y. Naraki, K. Ohara, S. Kohara, T. Okubo, T. Wakihara, Cryst. Growth Des. 16 (2016) 3389-3394.

[16]   H. Wang, B.A. Holmberg, Y. Yan, J. Am. Chem. Soc. 125 (2003) 9928-9929.

[17]   E.-P. Ng, G.K. Lim, G.-L. Khoo, K.-H. Tan, B.S. Ooi, F. Adam, T.C. Ling, K.-L. Wong, Mater. Chem. Phys. 155 (2015) 30-35.

[18]   Y. Wang, Q. Wu, X. Meng, F.-S. Xiao, Engineering 3 (2017) 567-574.

[19]   Y. Kamimura, W. Chailittisilp, K. Itabashi, A. Shimojima, T. Okubo, Chem. Asian J. 5 (2010) 2182-2191.

[20]   E.-P. Ng, H. Awala, J.-P. Ghoy, A. Vicente, T.C. Ling, Y.H. Ng, S. Mintova, F. Adam, Mater. Chem. Phys. 159 (2015) 38-45.

[21]   H. Awala, J.P. Gilson, R. Retoux, P. Boullay, J.M. Goupil, V. Valtchev, S. Mintova, Nat. Mater. 14 (2015) 447-451.

[22]   V.P. Valtchev, K.N. Bozhilov, J. Phys. Chem. B 108 (2004) 15587-15598.

[23]   J. Kecht, B. Mihailova, K. Karaghiosoff, S. Mintova, T. Bein, Langmuir 20 (2004) 5271–5276.

[24]   V.P. Valtchev, L. Tosheva, K.N. Bozhilov, Langmuir 21 (2005) 10724-10729.

[25]   M. Tsapatsis, T. Okubo, M. Lovallo, M.E. Davis, Mat. Res. Soc. Symp. Proc. 371 (1995) 21-26.

[26]   Y. Liu, M. Sun, C.M. Lew, J. Wang, Y. Yan, Adv. Funct. Mater. 18 (2008) 1732-1738.

[27]   Y.-W. Cheong, K.-L. Wong, T.C. Ling, E.-P. Ng, Mater. Express 8 (2018) 1-6.

[28]   K. Jiao, X. Xu, Z. Lv, J. Song, M. He, H. Gies, Micropor. Mesopor. Mater. 225 (2016) 98-104.

[29]   T. Kurniawan, O. Muraza, K. Miyake, A.S. Hakeem, Y. Hirota, A.M. Al-Amer, N. Nishiyama, Ind. Eng. Chem. Res. 56 (2017) 4258-4266.

[30]   W. Fan, K. Morozumi, R. Kimura, T. Yokoi, T. Okubo, Langmuir 24 (2008) 6952-6958.

[31]   E.-P. Ng, L. Delmotte, S. Mintova, Green Chem. 10 (2008) 1043-1048.

[32]   E.-P. Ng, K.-L. Wong, D.T.-L. Ng, H. Awala, R.R. Mukti, F. Adam, S. Mintova, Mater. Chem. Phys. 188 (2017) 49-57.

[33]   G. Majano, K. Raltchev, A. Vicente, S. Mintova, Nanoscale 7 (2015) 5787-5793.

[34]   X. Chen, D. Xi, Q. Sun, N. Wang, Z. Dai, D. Fan, V. Valtchev, J. Yu, Micropor. Mesopor. Mater. 234 (2016) 401-408.

[35]   R.M. Barrer, E.A.D. White, J. Chem. Soc. (1951) 1267.

[36]   IZA-SC Database of Zeolite Structures. http://www.iza-structure.org/ databases/.

[37]   P. Norby, A. Nørlund Christensen, I. G. Krogh Andersen, Acta Chem. Scand. A40 (1986) 500.

[38]   R. Klaska, O. Jarchow, Naturwiss. 60 (1973) 299.; R. Klaska, O. Jarchow, Z. Kristallogr. 142 (1975) 225-238.

[39] G.D. Gatta, N. Rotiroti, P.F. Zanazz, M. Rieder, M. Drabek, Z. Weiss, R. Klaska, Am. Mineral. 93 (2008) 988-995.

[40] G.D. Gatta, M. Merlini, P. Lotti, A. Lausi, M. Rieder, Micropor. Mesopor. Mater. 163 (2012) 147-152.

[41] D. Massiot, F. Fayon, M. Capron, I. King, S. Le Calvé, B. Alonso, J.-L. Durand, B. Bujoli, Z. Gan, G. Hoatson, Magn. Reson. Chem. 40 (2002) 70-76.

[42] H. Maghsoodloorad, S.M. Mirfendereski, T. Mohammadi, A. Pak, Clay Clay Miner 59 (2011) 328-335.

[43] J.-L. Guth, H. Kessler, in: J. Weitkamp, L. Puppe (Eds.), Catalysis and Zeolites: Fundamentals and Applications, Springer-Verlag, Berlin, 1999, pp. 20-21.

[44] HG. Liu, Q. Shi, L. Liu, H. Xu, J. Li and J. Dong, Stud. Surf. Sci. Catal. 174A (2008) 185-188.

[45] K. Spektor, A. Fischer, U. Haussermann, Inorg. Chem. 55 (2016) 8048-8058.

[46] S.-F. Wong, H. Awala, A. Vincente, R. Retoux, T.C. Ling, S. Mintova, R.R. Mukti, E.-P. Ng, Micropor. Mesopor. Mater. 249 (2017) 105-110.

[47] P. Guo, Structure Determination and Prediction of Zeolites, PhD thesis, Stockholm University, 2016, 73.

[48] Ch. Baerlocher, W.M. Meier, D.H. Olson, Atlas of Zeolite Framework Types, Elsevier, Amsterdam, 2001, pp. 26–27.

[49] L Itani, Y Liu, W Zhang, KN Bozhilov, L Delmotte, V Valtchev, J. Am. Chem. Soc. 131 (2009) 10127-10139.

[50] V.P. Valtchev, K.N. Bozhilov, J. Am. Chem. Soc. 127 (2005) 16171-16177.

[51] G. Engelhardt, Stud. Surf. Sci. Catal. 137 (2001) 387-418.

Graphical abstract

- Organic template free
- Fast synthesis
- Low pressure
- Low temperature
- High solid yield
- Si/Al ratio = 1.0

Cs-ABW

Research highlights

- Cs-ABW zeolite is prepared under low temperature (180 °C) and pressure (22 bar).

- The synthesis condition is much safer and faster than that of previous works.

- The nucleation and crystallization of nanozeolites in template-free hydrogel are studied.

- Fully crystalline Cs-ABW nanocrystals are formed after 120 min.

- The crystals (ca. 32 nm, Si/Al = 1.0) have grain shape morphology.

- High solid yield offering large-scale production of highly basic zeolite nanoparticles.

Figure captions

Fig. 1. Yield of solids recovered after different time intervals of hydrothermal synthesis.

Fig. 2. XRD patterns of samples after heating for (a) 10 min, (b) 17 min, (c) 30 min, (d) 60 min and (e) 120 min. The theoretical XRD pattern reported in ref. [39] is shown in (f).

**Fig. 3.** Degree of crystallinity of samples after heating for various times.

Fig. 4. TEM images of samples collected after hydrothermal treatment for (a, b) 10 min, (c, d) 17 min, (e, f) 30 min and (g, h) 120 min.

Fig. 5. FTIR spectra of the solid after hydrothermal treatment for (a) 10 min, (b) 17 min, (c) 30 min and (d) 120 min.
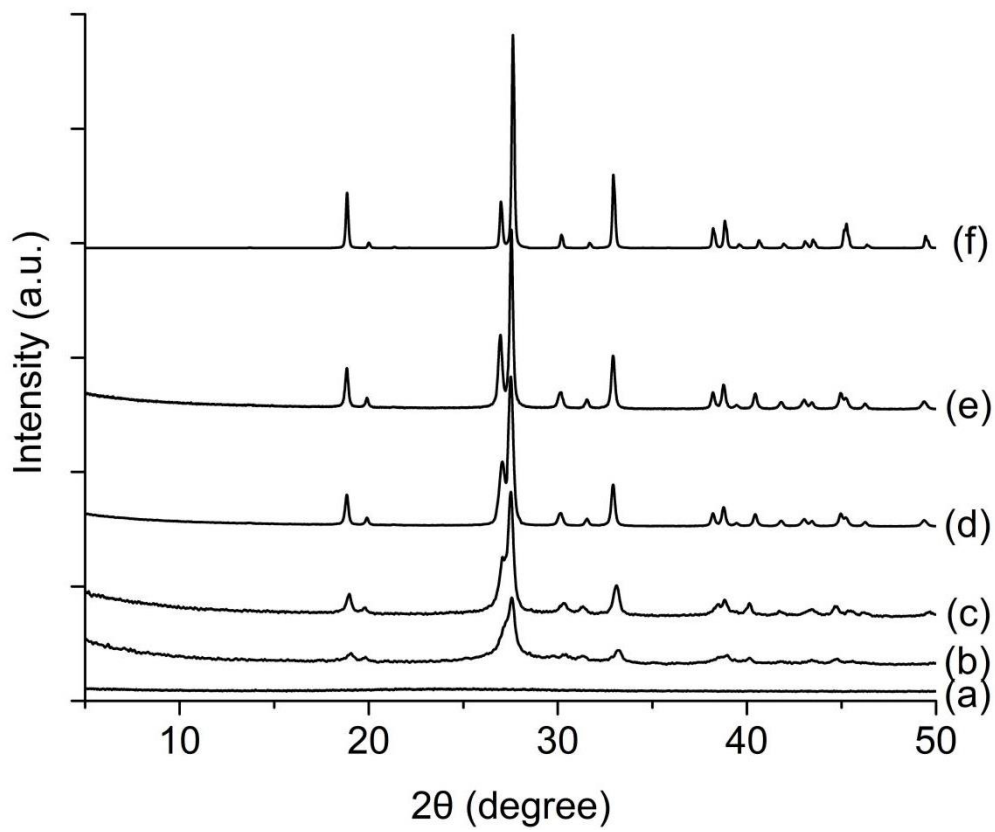
Fig. 6. ^{27}Al solid state MAS NMR spectra of the solid after hydrothermal treatment for (a) 10 min, (b) 17 min, (c) 30 min and (d) 120 min.

Fig. 7. ^{28}Si MAS + DEC NMR spectra of the solid samples after hydrothermal treatment for (a) 10 min, (b) 17 min, (c) 30 min and (d) 120 min.
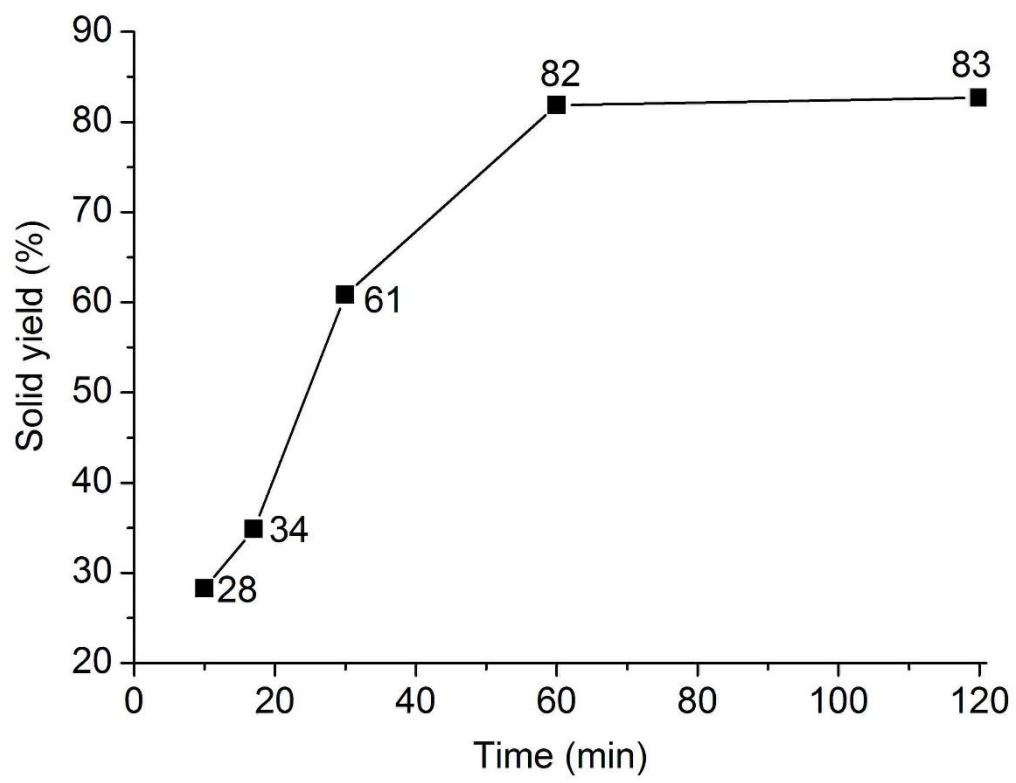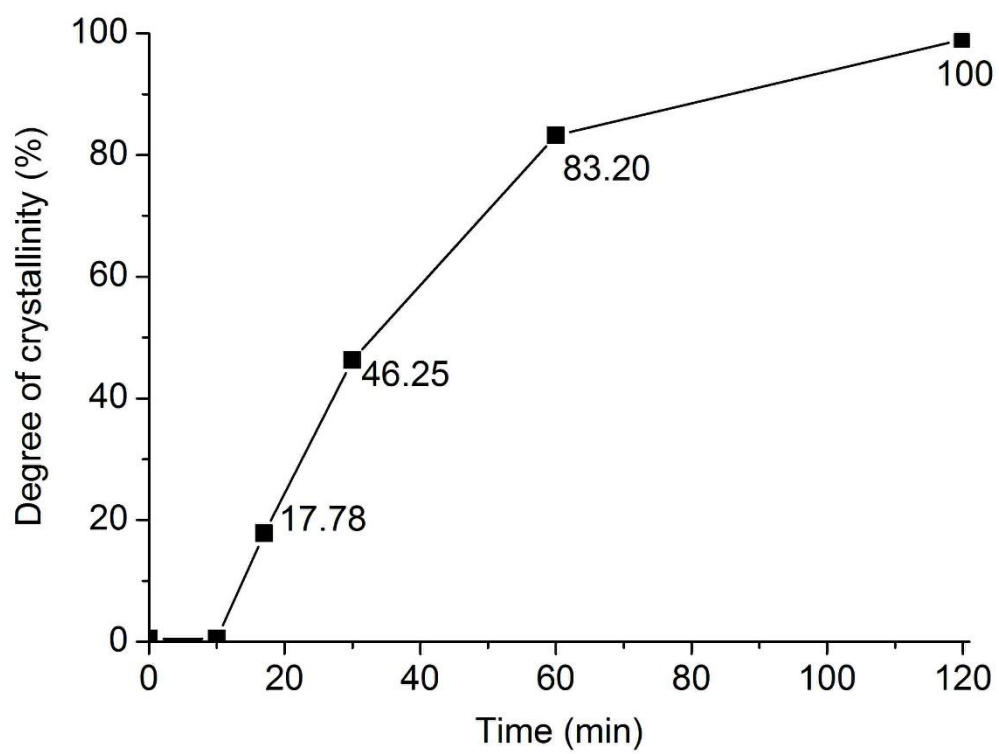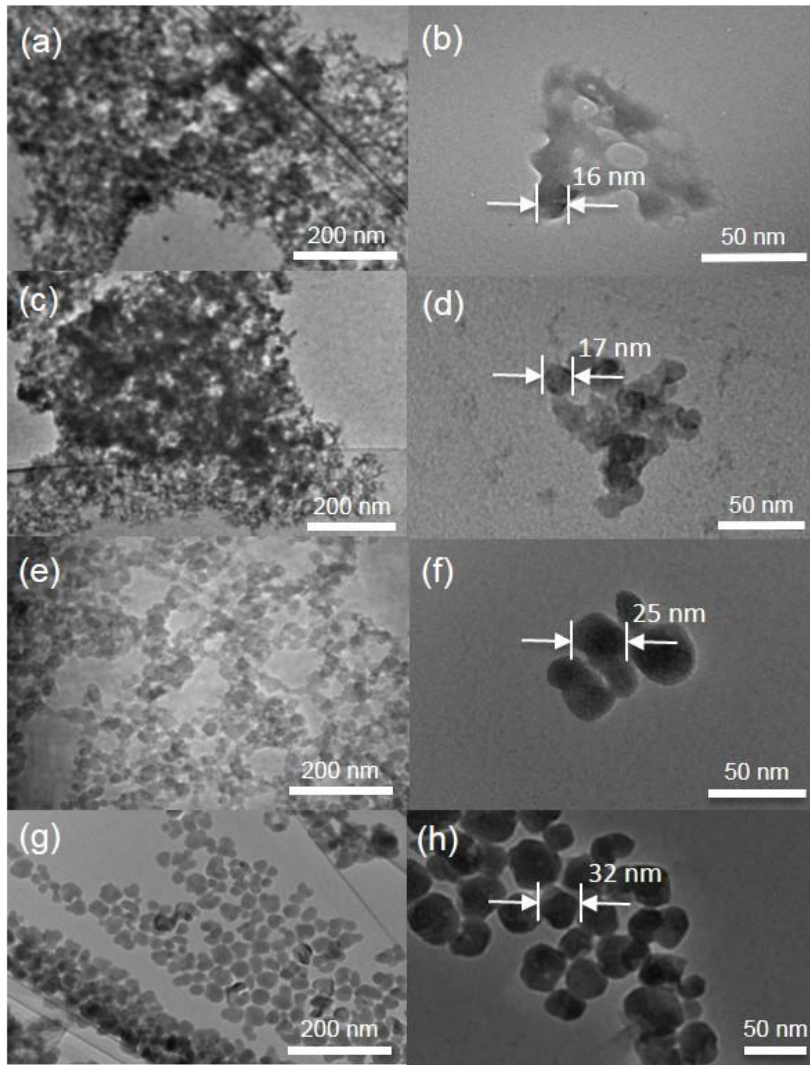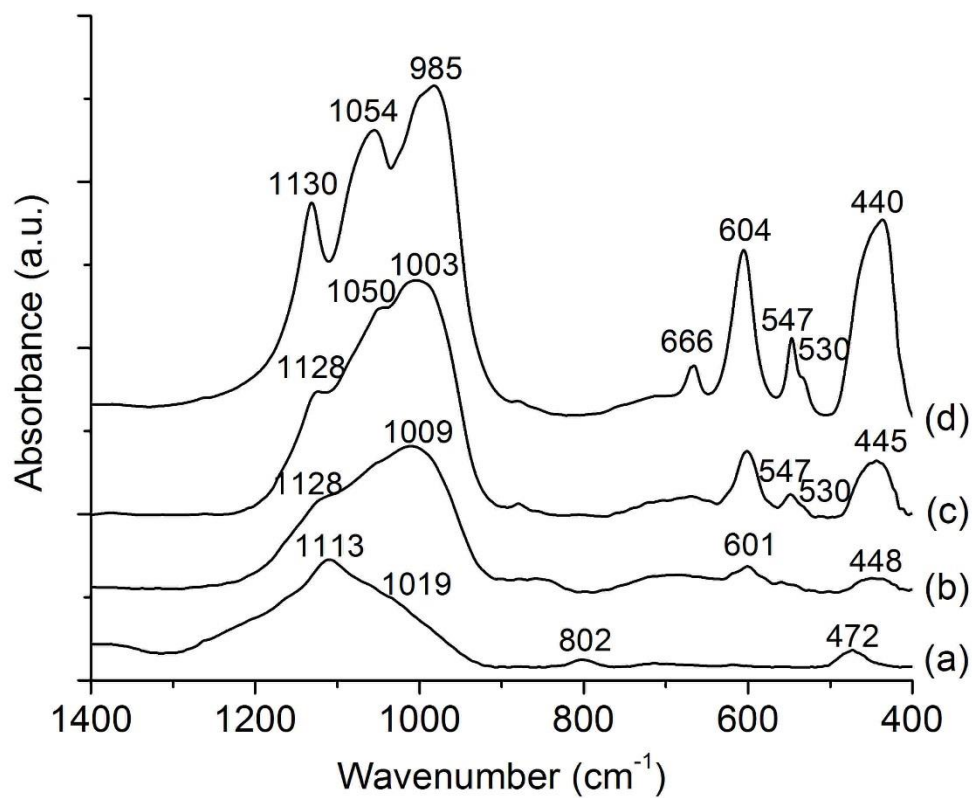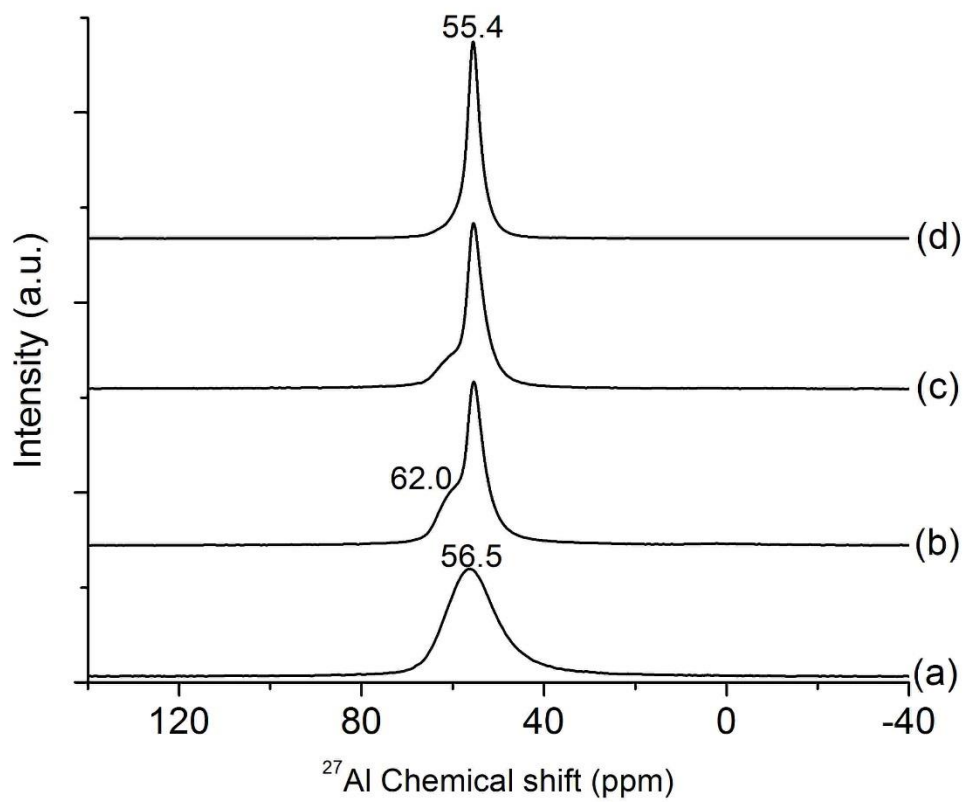
Fig. 1.

Fig. 2.
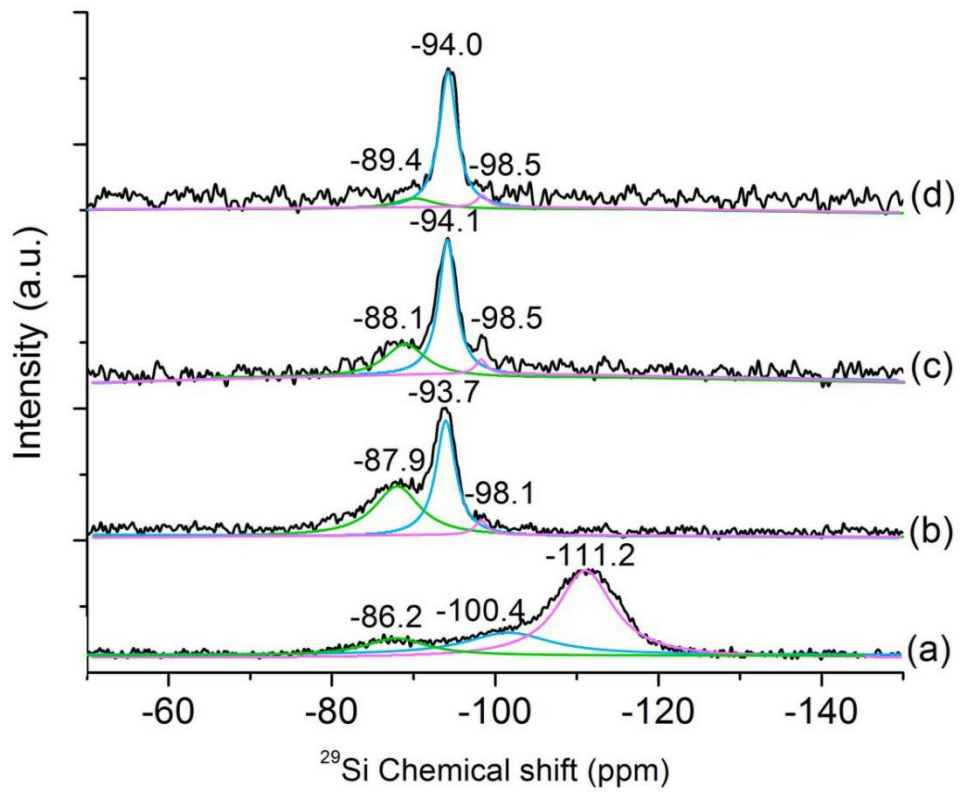
Fig. 3.

Fig. 4.

Fig. 5.

Fig. 6.

Fig. 7.

Tables

Table 1. Synthesis conditions and characteristics of solid products obtained from hydrothermal syntheses.

Variable parameters	Entry	Gel molar composition				T (°C)	t (min)	Products[a]
		SiO₂	**Al₂O₃**	**Cs₂O**	**H₂O**			
Cs₂O	1	4	1	8	164	180	80	Am.
	2			12				ABW (41)
	3			16				ABW (26)
H₂O	4	4	1	16	124	180	80	ABW (19)
	3				164			ABW (26)
	5				204			ABW (44)
SiO₂/Al₂O₃ ratio	6	2	1	16	164	180	80	ABW (34)
	3	4						ABW (26)
	7	6						Am.
Metal hydroxide	9	4	1	16 Na₂O	164	180	80	CAN (57)
	10			16 K₂O				LTJ (94)
	3			16 Cs₂O				ABW (26)
Temperature	11	4	1	16	164	140	80	Am.
	12					160		Am. > ABW (16)
	3					180		ABW (26)
Time	13	4	1	16	164	180	10	Am.
	14						17	Am. >> ABW (15)
	15						30	Am. > ABW (21)
	16						60	ABW (25) > Am.
	17						120	ABW (28)

Table 2. Chemical elemental analysis of the solid products obtained after various heating times.

Samples	Si		Al		Cs		Si/Al ratio	Cs/Al ratio
	mg/L	mmol/L	mg/L	mmol/L	mg/L	mmol/L		
10 min	318.9	11.39	27.3	1.01	46.1	0.35	11.28	0.35
17 min	165.0	5.89	83.9	3.10	303.8	2.29	1.90	0.74
30 min	110.9	3.96	85.0	3.15	402.8	3.03	1.25	0.95
120 min	90.1	3.22	85.1	3.15	441.8	3.32	1.02	1.05